NASA/TM-1999-209141
ARL-TR-2000

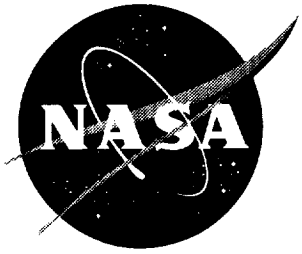

Quasi-Static Viscoelastic Finite Element Model of an Aircraft Tire

Arthur R. Johnson
U.S. Army Research Laboratory
Vehicle Technology Directorate
Langley Research Center, Hampton, Virginia

John A. Tanner
Boeing Commercial Airplane Group, Seattle, Washington

Angela J. Mason
Langley Research Center, Hampton, Virginia

National Aeronautics and
Space Administration

Langley Research Center
Hampton, Virginia 23681-2199

April 1999

Available from:

NASA Center for AeroSpace Information (CASI)
7121 Standard Drive
Hanover, MD 21076-1320
(301) 621-0390

National Technical Information Service (NTIS)
5285 Port Royal Road
Springfield, VA 22161-2171
(703) 605-6000

QUASI-STATIC VISCOELASTIC FINITE ELEMENT MODEL OF AN AIRCRAFT TIRE

Arthur R. Johnson[#], John A. Tanner[†], and Angela J. Mason[‡]

Computational Structures Branch, MS240
NASA Langley Research Center
Hampton, VA 23681-0001

ABSTRACT

An elastic large displacement thick-shell mixed finite element is modified to allow for the calculation of viscoelastic stresses. Internal strain variables are introduced at the element's stress nodes and are employed to construct a viscous material model. First order ordinary differential equations relate the internal strain variables to the corresponding elastic strains at the stress nodes. The viscous stresses are computed from the internal strain variables using viscous moduli which are a fraction of the elastic moduli. The energy dissipated by the action of the viscous stresses is included in the mixed variational functional. The nonlinear quasi-static viscous equilibrium equations are then obtained. Previously developed Taylor expansions of the nonlinear elastic equilibrium equations are modified to include the viscous terms. A predictor-corrector time marching solution algorithm is employed to solve the algebraic-differential equations. The viscous shell element is employed to computationally simulate a stair-step loading and unloading of an aircraft tire in contact with a frictionless surface.

Army Research Laboratory, Vehicle Technology Directorate, MS240.
† Boeing Commercial Airplane Group, Seattle, WA.
‡ Structural Dynamics Branch, MS497.

INTRODUCTION

Aircraft tires are composite structures manufactured with viscoelastic materials such as carbon black filled rubber and nylon cords. When loaded, tires experience large deflections and moderately large strains.[1] Finite element models of tires typically employ either two-dimensional thick shell or three-dimensional solid elements.[2,3] Elastic finite element shell models for tires have been used to predict the shape of tire footprints as a function of loading.[4-9] Elastic models do not include the viscoelastic nature of the tire which can have a significant effect on load-displacement curves. This study is the computational part of an effort in which the quasi-static viscoelastic loading and unloading of an aircraft tire was measured and computationally simulated. The experimental effort and the load measurements have been reported elsewhere.[10]

In several previous studies viscoelastic constitutive models have been utilized to determine the dynamic deformations of tires. The following references are provided as a starting point for readers interested in obtaining details about other viscoelastic finite element models for tires. Padovan, et al.[11,12,13] performed an extensive study in which a finite element algorithm was developed for rolling tires. Padovan's model included the effects of large deformations and contact. It also employed fractional derivatives to model the viscoelastic effects. The tire models made by Oden et al.[2,3] also included the effects of large deformations and contact. However, Oden's model employed the history integral formulation for the viscoelastic effects.

In this report, internal strain variables are employed to convert an elastic mixed shell element[4] into a viscous mixed shell element. The model is developed as follows. Internal strain variables are introduced at the stress nodes of the mixed element. First order differential equations relate the internal variables

to the physical strain variables. The equations represent a Maxwell solid.[14,15] Viscous stresses are determined from the internal strains by using material parameters referred to as viscous moduli. An expression for the energy dissipated during deformation is computed from the viscous stresses. This is accomplished by employing the finite element interpolations that are used to compute the elastic stresses from the elastic strains in the elastic version of the shell element. The dissipation energy functional is added to the mixed variational statement for the elastic problem. Nonlinear algebraic equilibrium equations are determined and are numerically solved, simultaneously, with the internal variable differential equations. The numerical solution procedure employs the Newton-Raphson method for the nonlinear algebraic equations, and the trapezoidal method for the differential equations in a predictor-corrector combination. The tangent matrix required in the Newton-Raphson scheme is a modified version of the previously determined[4,7-9] tangent matrix for the nonlinear elastic problem.

At the end of the paper, the viscous shell element is employed in a computational simulation of a stair-step loading and unloading of an aircraft tire. The elastic material constants used are from a previous effort.[7] The viscous material constants required are estimated by making a least-squares fit of load-relaxation data, as predicted by a one-dimensional version of the viscous model, to measured load-relaxation data. In the simulation, the stair-step tire rim displacement, as measured in the experimental effort,[10] is enforced. The computed and measured stair-step hysteresis curves are presented together for reference.

VISCOELASTIC MIXED SHELL ELEMENT

An elastic shell element capable of modeling geometrically nonlinear deformations of thick laminated composites was developed

by Noor, et al.[4-9] Figure 1. shows the physical variables employed to describe the energy in the deformed shell. The elastic finite element has nine displacement nodes with five variables at each node, and four stress nodes with eight variables at each node, see Figure 2. The constitutive model[7-9] in the shell generalized coordinates is abbreviated as

$$\sigma = \mathbf{C}\,\mathbf{e} \tag{1}$$

where $\sigma = \left(N_s, N_\theta, N_{s\theta}, M_s, M_\theta, M_{s\theta}, Q_s, Q_\theta\right)^T$ is a vector of stress variables, $\mathbf{e} = \left(\varepsilon_s, \varepsilon_\theta, 2\varepsilon_{s\theta}, \kappa_s, \kappa_\theta, 2\kappa_{s\theta}, 2\varepsilon_{s3}, 2\varepsilon_{\theta 3}\right)^T$ is a vector of the Sanders-Budiansky[19,20] nonlinear strains, and $\mathbf{C}$ is a matrix of elastic stiffness constants. The elastic element employs the Hellinger-Resiner mixed variational principle which is constructed as follows. The complementary form of the energy is integrated over the volume of the shell and the total work done by external forces is subtracted. This results in π_{HR} which is expressed as follows.

$$\pi_{HR} = \int_\Omega \left(\sigma^{\mathrm{T}} \mathbf{e} - \frac{1}{2} \sigma^{\mathrm{T}} \mathbf{F}\, \sigma \right) d\Omega - W \tag{2}$$

where Ω is the volume of the shell, $\mathbf{F}$ is a flexibility matrix, and W is the work done by external forces.

Next, the energy functional, π_{HR}, is discretized by the finite element method.[4] At the element level, the displacements and stress resultants are approximated by employing interpolation functions with the nodal values shown in Figure 2. The Sanders-Budiansky nonlinear strains are computed and substituted into Equation (2) above. After the volume integration is performed for an element, the Hellinger-Resiner variational expression is given in short-hand notation as follows.

$$\pi_{HR}^{elt}(\mathbf{x},\mathbf{h}) = V - U^C - W \tag{3}$$

where $V = \int_{\Omega_{elt}} \sigma^{\mathrm{T}} \mathbf{e}\, d\Omega \equiv \hat{\mathbf{h}}^{\mathrm{T}} \left(\hat{\mathbf{S}}_{\ell x} + \frac{1}{2} \hat{\mathbf{M}}_{n\ell xx} \right) \equiv \hat{\mathbf{h}}^{\mathrm{T}} \hat{\mathbf{e}}$,

$U^C = \int_{\Omega_{elt}} \frac{1}{2} \sigma^{\mathrm{T}} \mathbf{F}\, \sigma\, d\Omega \equiv \frac{1}{2} \hat{\mathbf{h}}^{\mathrm{T}} \hat{\mathbf{F}}\, \hat{\mathbf{h}}$, $W = \hat{\mathbf{x}}^{\mathrm{T}} \hat{\mathbf{p}} = \hat{\mathbf{p}}^{\mathrm{T}} \hat{\mathbf{x}}$, $\hat{\mathbf{x}}$ and $\hat{\mathbf{e}}$ are vectors containing the element's nodal displacements and strains, $\hat{\mathbf{h}}$ is an element level vector, $\hat{\mathbf{S}}_{\ell x}$ and $\hat{\mathbf{M}}_{n\ell xx}$ are operators that produce the linear and nonlinear contributions to $\hat{\mathbf{e}}$ from the nodal displacements, $\hat{\mathbf{F}}$ is an element level flexibility matrix, and $\hat{\mathbf{p}}$ represents the consistent applied load vector.

Internal strain variables are employed herein to modify the above formulation making it applicable to a Maxwell type viscoelastic material.[14,15] Introduce, in vector form, internal strain fields, $\mathbf{e}_{jv}$, and matrices of viscous stiffness constants, $\mathbf{C}_v$, within the element. The viscous stress vector at a point in the element is computed as follows.

$$\sigma_v = \sum_{j=1}^{n} \mathbf{C}_v \mathbf{e}_{jv} \tag{4}$$

The total value of the stress vector, elastic plus viscous, at a point is $\sigma_t = \sigma + \sigma_v$. Next, following the computation of the elastic potential, V, in Equation (3), the energy dissipated by the viscous stresses, Q, throughout the element is computed as follows.

$$Q = \int_{\Omega_{elt}} \sigma_v^{\mathrm{T}} \mathbf{e}\, d\Omega \equiv \hat{\mathbf{h}}_v^{\mathrm{T}} \hat{\mathbf{e}} = \hat{\mathbf{h}}_v^{\mathrm{T}} \left(\hat{\mathbf{S}}_{\ell x} + \frac{1}{2} \hat{\mathbf{M}}_{n\ell xx} \right) \tag{5}$$

where $\hat{\mathbf{h}}_v$ is an element level vector. The mixed variational functional for the viscous element, $\pi_{HR}^{elt,v}$, is given by

$$\pi_{HR}^{elt,v}\left(\hat{\mathbf{x}},\hat{\mathbf{h}}\right) = V + Q - U^C - W \tag{6}$$

The model is completed by relating the rate of change of the internal strain variables to the physical strain variables. Here we employ a simple form of the Maxwell solid theory by requiring the following differential equations to be satisfied.[14,15,18]

$$\frac{d\hat{\mathbf{e}}_{jv}}{dt} + \frac{\hat{\mathbf{e}}_{jv}}{\tau_{jv}} = \frac{d\hat{\mathbf{e}}}{dt} \qquad j = 1,2,\bullet\bullet\bullet,n \tag{7}$$

Equations (4) and (7) determine the viscous stresses for a time dependent deformation of the element, $\hat{\mathbf{x}}(t)$. Note, an advantage of this algorithm is that a variety of viscoelastic models can be employed by simply changing Equation (7).

At each instant of time, the element equilibrium equations are given by the first variation of $\pi_{HR}^{elt,v}$, Equation (6). The equilibrium equations are

$$\mathbf{f}_{\hat{\mathbf{h}}}\left(\hat{\mathbf{x}},\hat{\mathbf{h}}\right) = \left(\hat{\mathbf{S}}_{\ell x} + \frac{1}{2}\hat{\mathbf{M}}_{n\ell xx}\right) - \hat{\mathbf{F}}\,\hat{\mathbf{h}} = \mathbf{0} \tag{8}$$

and

$$\mathbf{f}_{\hat{\mathbf{x}}}\left(\hat{\mathbf{x}},\hat{\mathbf{h}}\right) = \left(\hat{\mathbf{S}}_{\ell} + \hat{\mathbf{M}}_{n\ell x}\right)^{\mathrm{T}}\left(\hat{\mathbf{h}} + \hat{\mathbf{h}}_v\right) - \hat{\mathbf{p}} = \mathbf{0} \tag{9}$$

where $\hat{\mathbf{S}}_{\ell}$ and $\hat{\mathbf{M}}_{n\ell x}$ are the derivatives of the operators $\hat{\mathbf{S}}_{\ell x}$ and $\hat{\mathbf{M}}_{n\ell xx}$ with respect to the element displacement variables, $\hat{\mathbf{x}}$. Equations (8) and (9) are assembled by standard methods to obtain

the global equilibrium equations. The global equations are then solved simultaneously with Equation 7 (for all elements.)

The Taylor expansion of Equations (8) and (9) produces the element's tangent matrix. The resulting element level Newton-Raphson equations for the increments of the variables $\Delta\hat{\mathbf{h}}$ and $\Delta\hat{\mathbf{x}}$ are given below.

$$\begin{bmatrix} -\hat{\mathbf{F}} & \hat{\mathbf{S}}_\ell + \hat{\mathbf{M}}_{n\ell x} \\ \left(\hat{\mathbf{S}}_\ell + \hat{\mathbf{M}}_{n\ell x}\right)^T & \hat{\mathbf{M}}_{n\ell}\left(\hat{\mathbf{h}} + \hat{\mathbf{h}}_v\right) \end{bmatrix} \begin{Bmatrix} \Delta\hat{\mathbf{h}} \\ \Delta\hat{\mathbf{x}} \end{Bmatrix} = \begin{Bmatrix} \mathbf{f}_{\hat{\mathbf{h}}} \\ \mathbf{f}_{\hat{\mathbf{x}}} \end{Bmatrix} \tag{10}$$

where $\hat{\mathbf{M}}_{n\ell}$ is the second derivative of the operator $\hat{\mathbf{M}}_{n\ell xx}$ with respect to the nodal displacements. Equations (10) are assembled for all elements and solved to provide estimates of the variables increments across a time step. The new elastic strains at the end of the time step are computed at all stress nodes. The internal strain variables are then estimated at the end of the time step by employing the trapezoidal method to Equation (7). Next, global equilibrium is checked. If equilibrium is not satisfied the process is repeated. When equilibrium is satisfied the required output is computed and the time is advanced.

TIRE STAIR-STEP LOADING SIMULATION

The aircraft tire simulated below is a 32 x 8.8, type VII, bias-ply Shuttle nose-gear tire which has a 20-ply rated carcass and a maximum speed rating of 217 knots.[7-10] The tread pattern consists of three circumferential grooves and the rated inflation pressure is 320 psi. During the stair-step test,[10] the tire was inflated to 300 psi. The rated operating load for the tire is 15,000 pounds.

Elastic Material Model

The details of the tire's elastic material model are described by Tanner.[7] The tire is a cord-rubber composite and was treated as a laminated material. It was divided into seven regions in the direction of the meridian (from the center of the tread region to the rim.) Tire thickness, properties of the plies, etc. were measured and tabulated. Elastic constants were computed by the law of mixtures to obtain linear orthotropic stress-strain constitutive models for each layer. These properties were transformed to the shell coordinate system and integrated through the thickness of the shell elements.

Viscoelastic Material Model

One dimensional tire loading data[10] is employed below to obtain an approximation to the viscous material properties. Obtaining and analyzing time dependent multi-axial test data would result in a more accurate viscous material model than the model described in this study. The task of performing multi-axial stress-strain tests on coupons cut from the tire was beyond the scope of this effort. Below we describe how the measured one-dimensional load-relaxation data is least-squares fit to a simplified form of Equation (4).

When a material is rapidly deformed from a relaxed unstrained state into a deformed state in which the strains are held constant, we have a state of stress relaxation in the material. In this case, Equations (7) can be integrated. The solutions are substituted into Equation (4) and the following stress-relaxation equation for $\sigma_t(t)$ is obtained.

$$\sigma_t(t) = \left[\mathbf{C} + \mathbf{C}_v \sum_{n=1}^{N} \alpha_n e^{\frac{-t}{\tau_n}} \right] \mathbf{e}\left(t = 0^+\right) \tag{11}$$

where $\mathbf{e}\left(t = 0^+\right)$ is the initial value of the rapidly obtained strain state achieved.

Since the test data is one dimensional we can not determine the matrix $\mathbf{C}_v$. Here, $\mathbf{C}_v$ is assumed to be equal to the matrix $\mathbf{C}$ throughout the tire. With this assumption, Equation (11) becomes

$$\sigma_t(t) = \left[1 + \sum_{n=1}^{N} \alpha_n e^{\frac{-t}{\tau_n}}\right] \mathbf{C}\, \mathbf{e}\left(t = 0^+\right) \tag{12}$$

Note, modeling the tire with shell elements neglects three-dimensional effects (such as tread compression, bead-rim interaction, etc.) When this shell element tire model is suddenly pressed against a frictionless platform, Equation (12) implies that the total measured load on the platform will be given by

$$f(t) = \left[1 + \sum_{n=1}^{N} \alpha_n e^{\frac{-t}{\tau_n}}\right] f\left(t = 0^+\right) \tag{13}$$

where $f\left(t = 0^+\right)$ is the elastic part of the tire's load on the platform. The Prony series coefficients in Equation (13) are determined below by performing a constrained least-squares fit to measured tire load-relaxation data.

The classical procedure of inspecting the log(load) versus log(time) data curve for a load-relaxation test is used to select a range of time constants, $\left\{\tau_n\right\}_{n=1}^{N}$. The range selected must include the full spectrum of decay rates needed to model the relaxation curve. The error, $\phi\left(t_i\right)$, at time t_i is

$$\phi\left(t_i\right) = \hat{f}\left(t_i\right) - f\left(t_i\right) = \hat{f}\left(t_i\right) - \left[1 + \sum_{n=1}^{N} \alpha_n e^{\frac{-t_i}{\tau_n}}\right] f\left(t = 0^+\right) \tag{14}$$

where $\hat{f}(t_i)$ is the measured platform load at time t_i. The square of the error indicated by Equation (14) is added for all the data and is minimized with the constraint that the coefficients, α_n, be positive. That is, so that $\{\alpha_n \geq 0\}_{n=1}^{N}$. The algorithm employed to solve this constrained minimization problem is due to Rusin.[21] It was also used by Johnson and Quigley[22] as part of an algorithm which solves nonlinear frictionless contact problems.

The relaxation data shown in Figure 3 is from a 900 sec load-relaxation test. In the test, a large displacement of the tire's rim was rapidly enforced and then held approximately constant for 900 sec. The enforced displacement was selected[10] so that the total tire loading would be near 20,000 lbs. Inspection of the tire rim to platform displacement data indicated that the platform was moving slightly during the test. The elastic component of the load-relaxation data was adjusted, as described below, to correct for the platform drift.

The adjustment was accomplished as follows. Inspection of the data indicated that only 7% of the total loading is viscoelastic. This implied that 93% of the correction for the platform drift is due to the change in the elastic component of the load. A cubic polynomial was least-squares fit to the stair-step hysteretic loading and unloading data. The resulting cubic curve is shown in Figure 4. It passes through the thin quasi-static hysteresis loop, and is an approximation to the elastic load-displacement curve. The platform location at the start of the load-relaxation, 2.194 in, is a reference position from which the drift can be measured. The total relaxing load was adjusted by the computed difference in the elastic component of the load due to the platform drifting. The adjusted load-relaxation curve is shown in Figure 5. Note that the adjusted curve has more noise than the original curve. The noise is due to the fact that the platform displacement data does not contain as many significant digits as the platform load data. However, the least-squares fit

to the noisy adjusted data presented in Figure 5 indicates that the resulting adjustment is significant.

With $\{\tau_n\}_{n=1}^{3} = \{10, 100, 1000\}$, the constrained least-squares Prony series for the adjusted load-relaxation data is

$$f(t) = \left[1 + 0.01836\, e^{\frac{-t}{10}} + 0.01630\, e^{\frac{-t}{100}} + 0.03650\, e^{\frac{-t}{1000}} \right] * 18523 \qquad (15)$$

More accurate least-squares curve fits can be obtained with a larger number of time constants (spaced more closely, etc.) However, the use of a large number of time constants slows down the finite element algorithm. All of the calculations below were performed employing the Prony series represented by Equation (15).

Selection of Time Step

Prior to running the viscous version of the finite element code a one-dimensional numerical simulation of the stair-step test was made. The one-dimensional equations are solved quickly and produce insight on the size of the time steps required in the finite element simulation. A schematic of the one-dimensional material model is shown in Figure 6. The quasi-static equilibrium equations for the model are

$$\begin{aligned} f(t) &= f_e(x) + k_v \sum_{n=1}^{3} \alpha_j x_j \\ \frac{dx_j}{dt} + \frac{x_j}{\tau_j} &= \frac{dx}{dt} \quad for \;\; j = 1,2,3 \end{aligned} \qquad (16)$$

where $(\alpha_j, \tau_j)_{j=1}^{3}$ are the Prony series coefficients, $f_e(x)$ is the polynomial representation of the nonlinear elastic load displacement curve, $k_v = \dfrac{(\alpha_1 + \alpha_2 + \alpha_3) * 18523\ lbs}{2.194\ in}$ is the total

viscous stiffness obtained from the step strain relaxation data, and $\{x_j\}_{j=1}^{3}$ are the internal variables used to compute the viscous force.

A plot of the measured stair-step displacement data is shown in Figure 7. A piecewise linear representation of this curve was obtained by using straight lines between the corner points of the stair-steps. As noted above, close inspection of the data reveals that the platform was drifting during the relaxation intervals.

The simulation of the stair-step loading that results from integrating Equations (16) is shown in Figure 8. Load-displacement plots at the peak load, computed with time steps of 0.2 sec and 1.0 sec, are shown in Figure 9. The plots for each of these two time steps agree well. Smaller time steps did not provide any additional information. The values of the time constants, $\{\tau_n\}_{n=1}^{3}$, in the differential equations indicate that a time step of 2.0 sec or larger (to integrate $e^{\frac{-t}{10}}$ with the trapezoidal method) can be used. However, when a time step of 2.0 sec or larger was used, the errors introduced by missing the details of the stair-step ramping action were too large to accept. A time step of 1.0 sec was selected to for the finite element computations.

Finite Element Simulation

The tire's finite element mesh and a sketch of the loading platform are shown in Figure 10. The mesh is similar to the "Model 1" mesh employed by Tanner.[7] The elastic model has 540 elements and 28,565 degrees of freedom (not including the Lagrange multipliers used for points that come into contact.) An additional 103,680 internal variables were added to program the solution algorithm for the material model described above. The platform surface is frictionless. Computed elastic and viscoelastic load-displacement curves, obtained by enforcing the stair-step tire rim displacement are shown in Figure 11.

A comparison of the curves in Figures 8 and 11 indicates that the finite element model is stiffer than the one-dimensional model. This is because the elastic component of the finite element model is stiffer than the elastic component of the one-dimensional model. Since the one-dimensional model closely represents the measured data, the finite element model employed here produces a load-displacement curve which is above the measured data curve. The finite element load-displacement hysteresis loop and the measured hysteresis loop are shown in Figure 12. The measured loop encloses more area than the computed loop. This indicates that the simulation underestimated the viscous energy lost during the test.

CONCLUDING REMARKS

An algorithm for converting elastic structural elements based on the mixed Hellinger-Resiner mixed variational principle to viscoelastic structural elements was presented. The thirteen node large displacement thick-shell element derived by Noor and Hartley[4] was employed to describe the algorithm. A finite element tire model based on this shell element, and used by Tanner[7,8,9] to analyze tire footprints was modified so that the tire material would represent a Maxwell solid. Load-displacement data from a stair-step loading test was computationally simulated. The computed stair-step hysteresis loop indicated less viscous loss than the measured loop. The new computational algorithm functioned successfully. This algorithm can be applied to all structural elements of either displacement or mixed type.

ACKNOWLEDGMENT

The authors would like to thank Ms. Jeanne M. Peters of the Center for Advanced Computational Technology, University of Virginia, NASA Langley Research Center for assisting with the modifications of the finite element code.

REFERENCES

1. Clark, S. K., Ed., *Mechanics of Pneumatic Tires*, Chapter VII Tire Stress and Deformation, US Government Printing Office, Washington DC, pp 475-540, 1981.

2. Oden, J. T., Lin, T. L., and Bass, J. M., "A Finite Element Analysis of the General Rolling Contact Problem for a Viscoelastic Rubber Cylinder," Tire Science and Technology, TSTCA, Vol. 16, No. 1, pp 18-43, 1988.

3. Faria, L. O., Bass, J. M., Oden, J. T., and Becker, E. B., "A Three-Dimensional Rolling Contact Model for a Reinforced Rubber Tire," Tire Science and Technology, TSTCA, Vol. 17, No. 3, pp 217-233, 1989.

4. Noor, A. K. and Hartley, "Nonlinear Shell Analysis via Mixed Isoparametric Elements," Computers & Structures, Vol. 7, pp 615-626, 1977.

5. Noor, A. K., Anderson, C. M., and Tanner, J. A., "Exploiting Symmetries in the Modeling and Analysis of Tires," NASA Technical Paper 2649, March 1987.

6. Kim, K. O., Tanner, J. A., Noor, A. K., and Robertson, M. P., "Computational Methods for Frictionless Contact With Application to Space Shuttle Orbiter Nose-Gear Tires," NASA TP 3073, May 1991.

7. Tanner, J. A., "Computational Methods for Frictional Contact with Application to the Space Shuttle Orbiter Nose-Gear Tire, Comparisons of Experimental Measurements and Analytical Predictions," NASA TP 3573, May 1996.

8. Tanner, J. A., "Computational Methods for Frictional Contact with Application to the Space Shuttle Orbiter Nose-Gear Tire, Development of Frictional Contact Algorithm," NASA TP 3574, May 1996.
9. Tanner, J. A., V. J. Martinson, and M. P. Robinson, "Static Frictional Contact of the Space Shuttle Nose-Gear Tire," Tire Science and Technology, TSTCA, Vol. 22, No. 4, pp 242-272, 1994.
10. Mason, A. J., Tanner, J. A., and Johnson, A. R., "Quasi-Static Viscoelasticity Loading Measurements of an Aircraft Tire," NASA TM 4779, ARL TR 1402, NASA Langley Research Center, Hampton, VA, September 1997.
11. Padovan, J., "Finite Element Analysis of Steady and Transiently Moving/Rolling Nonlinear Viscoelastic Structure – I, Theory," Computers and Structures Vol. 27, No. 2, pp 249-257, 1987.
12. Kennedy, R., and Padovan, J., "Finite Element Analysis of Steady and Transiently Moving/Rolling Nonlinear Viscoelastic Structure – II, Shell and Three Dimensional Simulations," Computers and Structures Vol. 27, No. 2, pp 259-273, 1987.
13. Nakajima, Y., and Padovan, J., "Finite Element Analysis of Steady and Transiently Moving/Rolling Nonlinear Viscoelastic Structure – III, Impact/Contact Simulations," Computers and Structures Vol. 27, No. 2, pp 275-286, 1987.
14. Johnson, A. R. and Tessler, A., "A Viscoelastic Higher-order Beam Finite Element," in *The Mathematics of Finite Elements and Applications, Highlights 1996*, Wiley, Chichester, pp 333-345, 1997.
15. Johnson, A. R., Tessler, A., and Dambach, M. L., "Dynamics of Thick Viscoelastic Beams," ASME Journal of Engineering and Materials and Technology, Vol. 119, pp 273-278, 1997.
16. Ward, I. M., *Mechanical Properties of Solid polymers*, John Wiley & Sons, 1983.
17. Johnson, A. R. and Stacer, R. G., "Rubber Viscoelasticity using the Physically Constrained System's Stretches as Internal Variables," Rubber Chemistry and Technology, Vol. 66, No. 4, pp 567-577, 1993.

18. Johnson, A. R., "Modeling Viscoelastic Materials Using Internal Variables," The Shock and Vibration Digest, Vol. 31, No. 2, pp 91-100, 1999.
19. Sanders, J. L., Nonlinear Theories for Thin Shells, Q. Appl. Math., vol. 21, no. 1, pp 21-36, 1963.
20. Budiansky, B., Notes on Nonlinear Shell Theory, J. Appl. Mech., vol. 35, no. 2, pp 393-401, 1968.
21. Rusin, M. H., "A Revised Simplex Method for Quadratic Programming," SIAM J. Appl. Math., Vol. 20, pp 143-160, 1971.
22. Johnson, A. R. and Quigley, C. J., "Frictionless Geometrically Non-Linear Contact Using Quadratic Programming," Int. J. for Numerical Methods in Engineering, Vol. 28, pp 127-144, 1989.

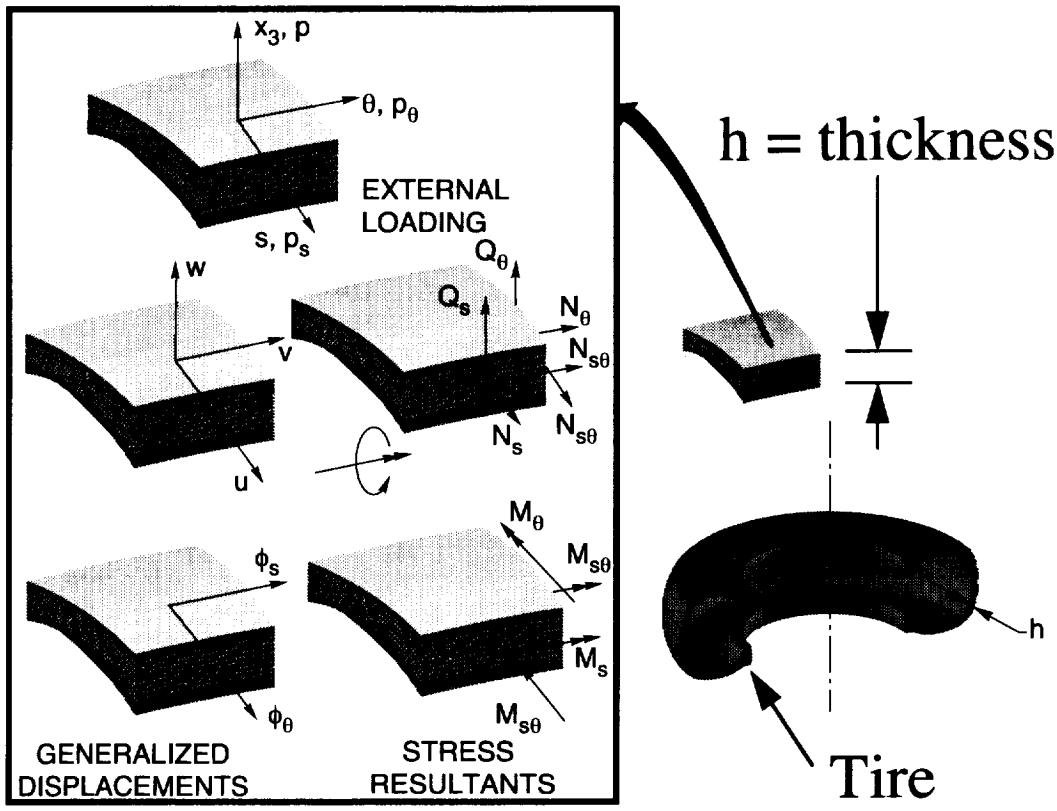

Figure 1. Shell displacement and force variables.

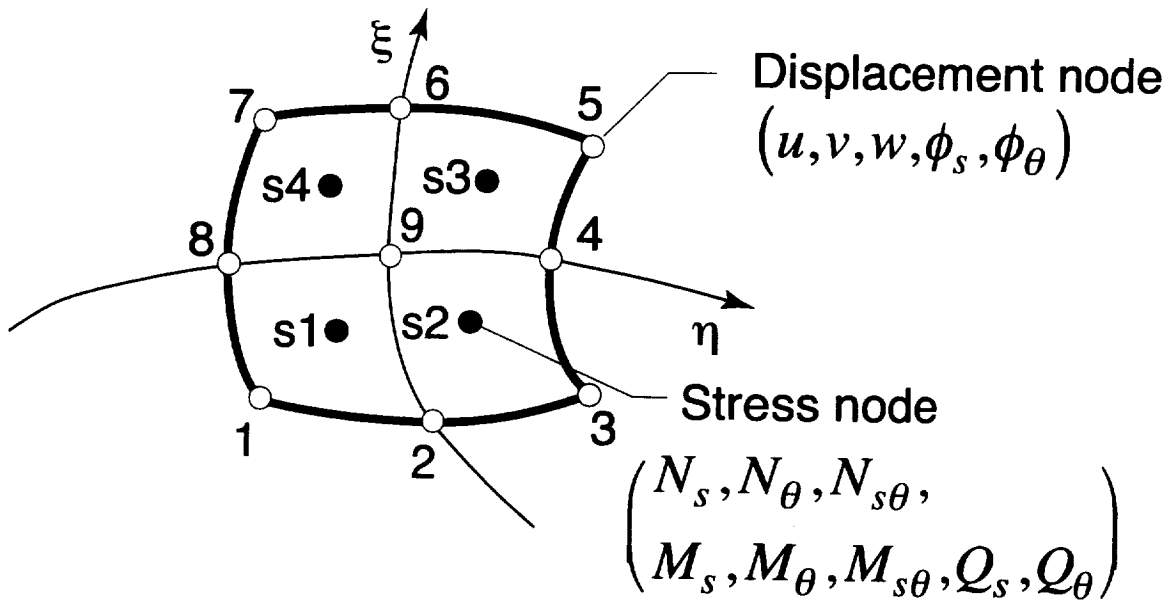

Figure 2. Shell finite element displacement and stress nodal variables.

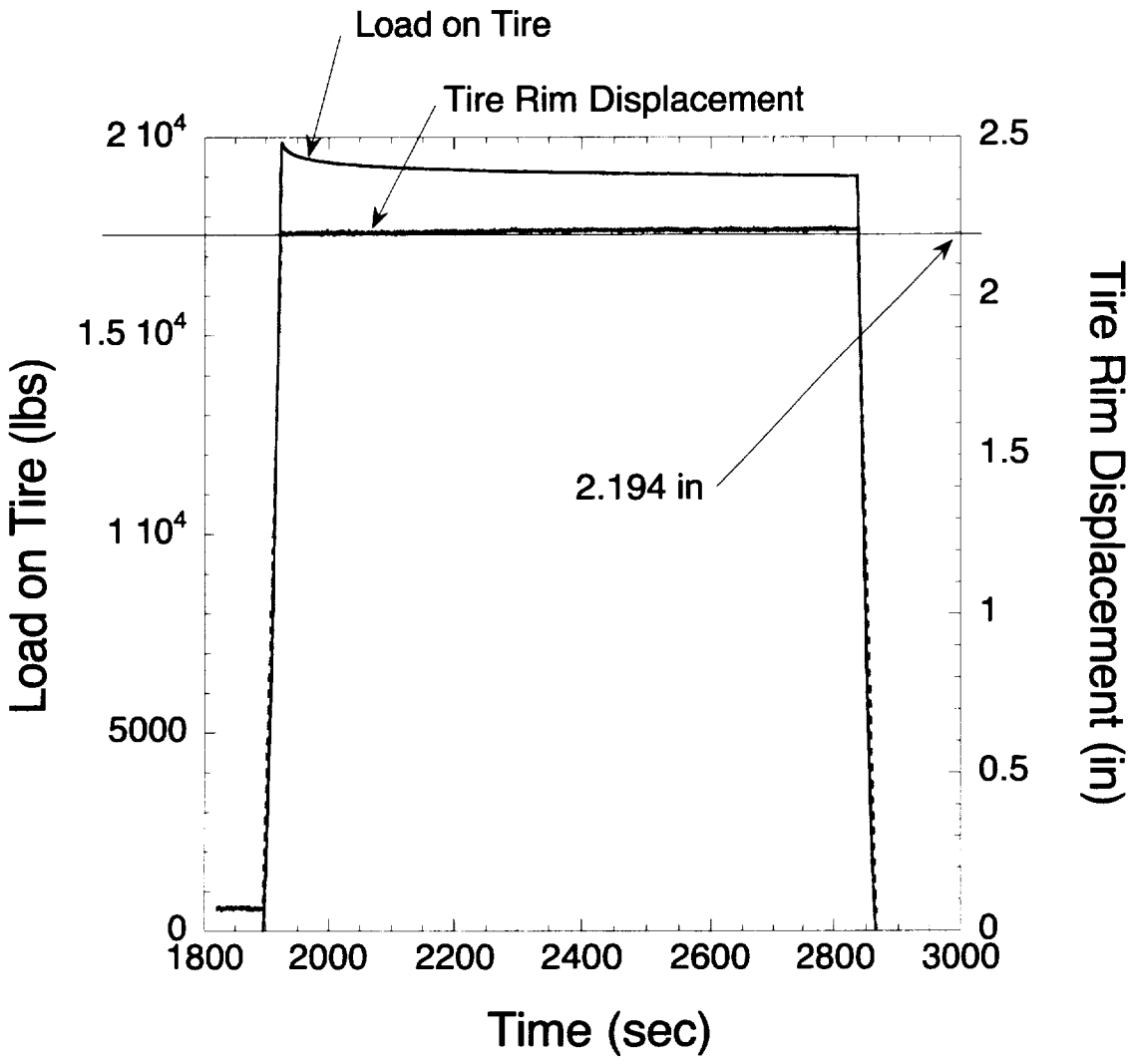

Figure 3. Tire load-relaxation and rim displacement data.

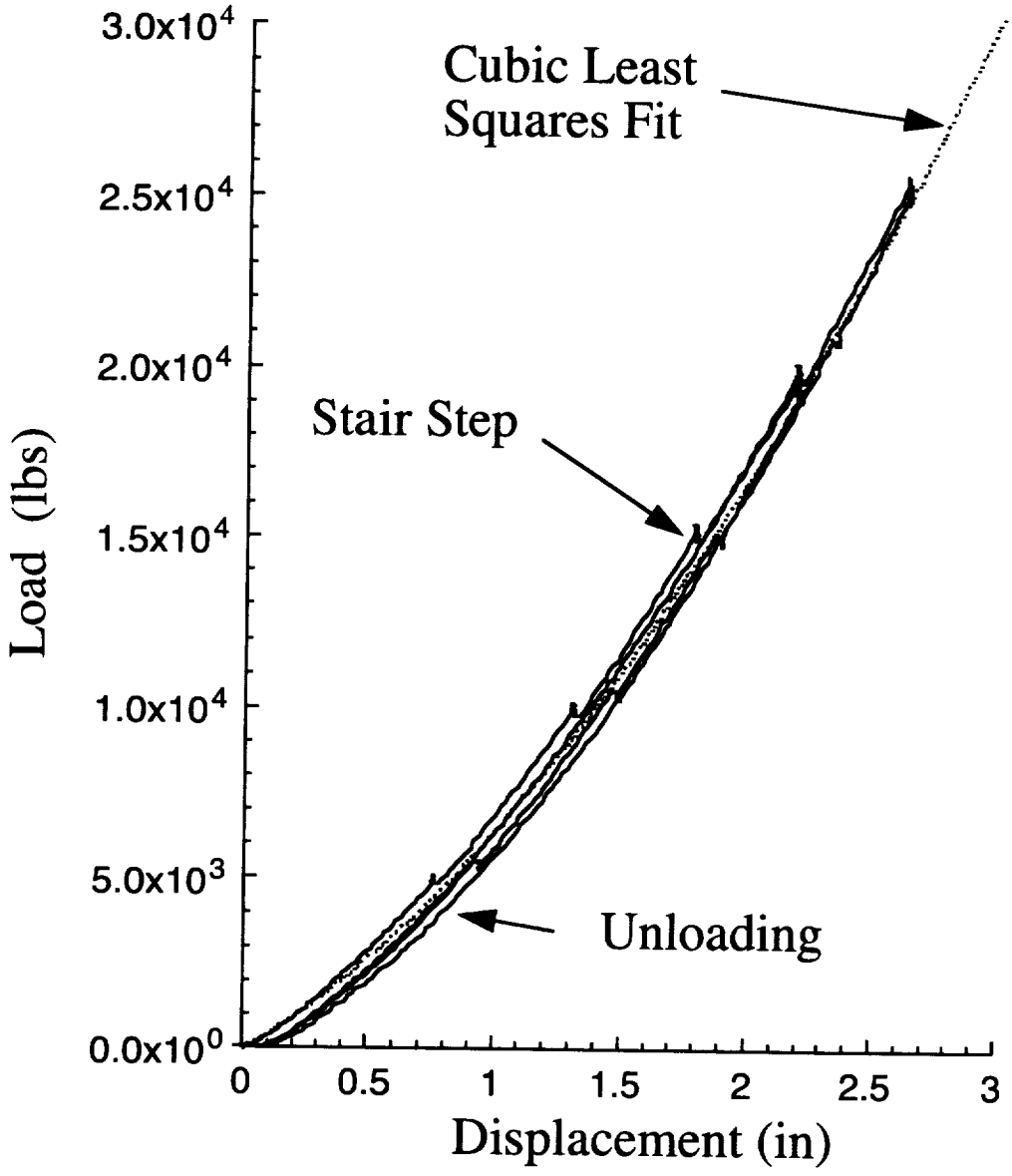

Figure 4. Tire stair-step loading data.

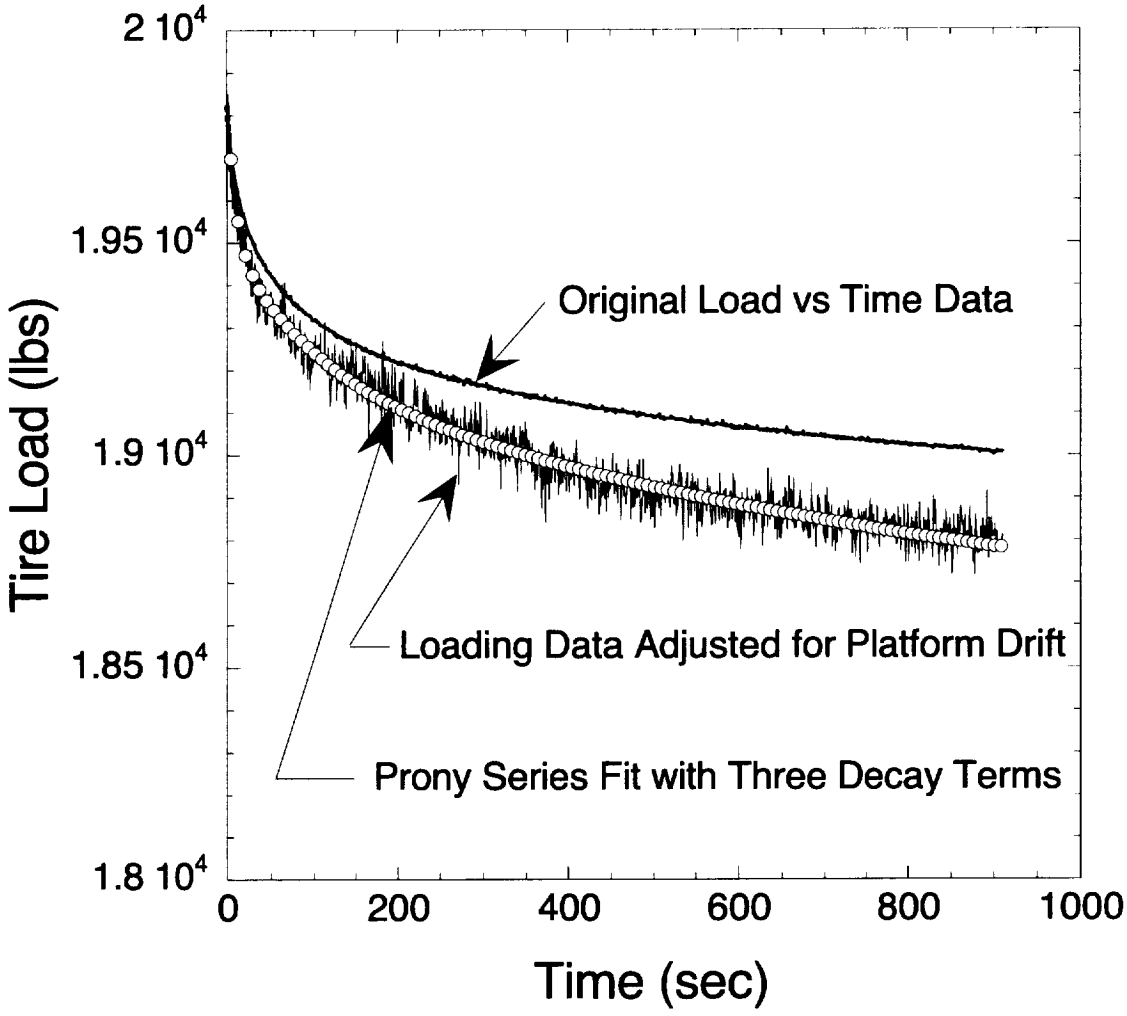

Figure 5. Adjusted tire load-relaxation data.

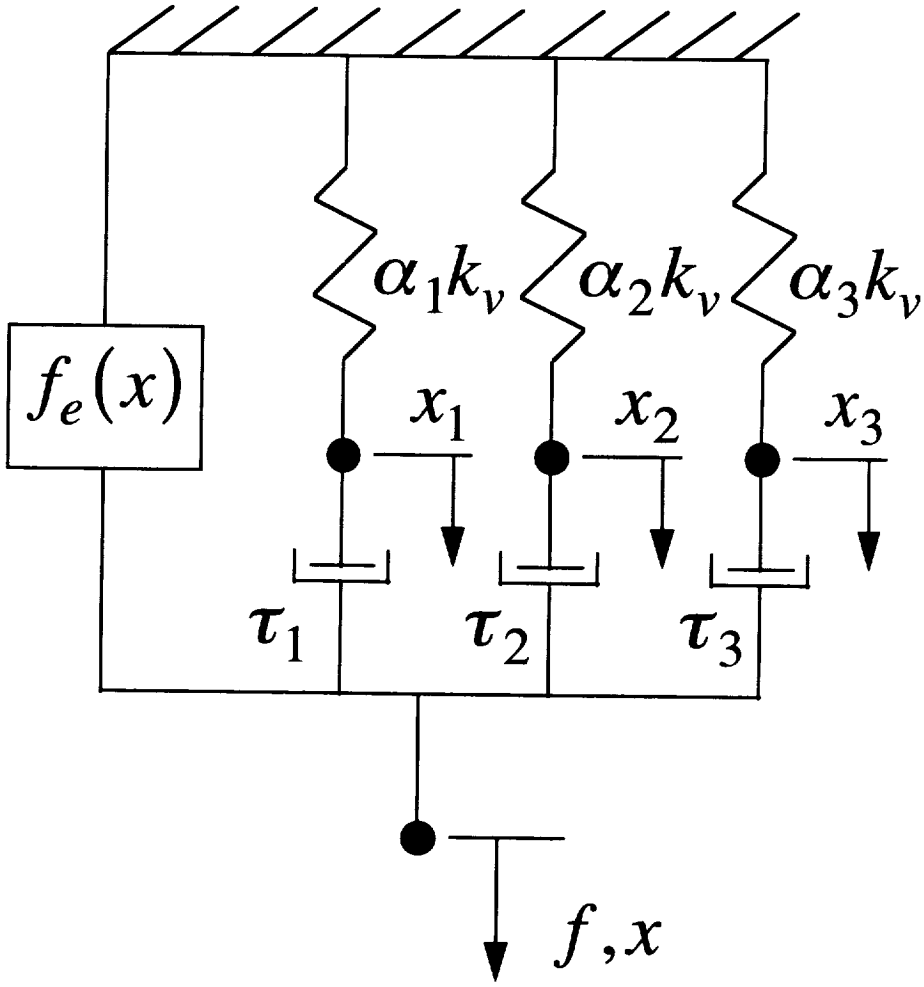

Figure 6. One dimensional material model.

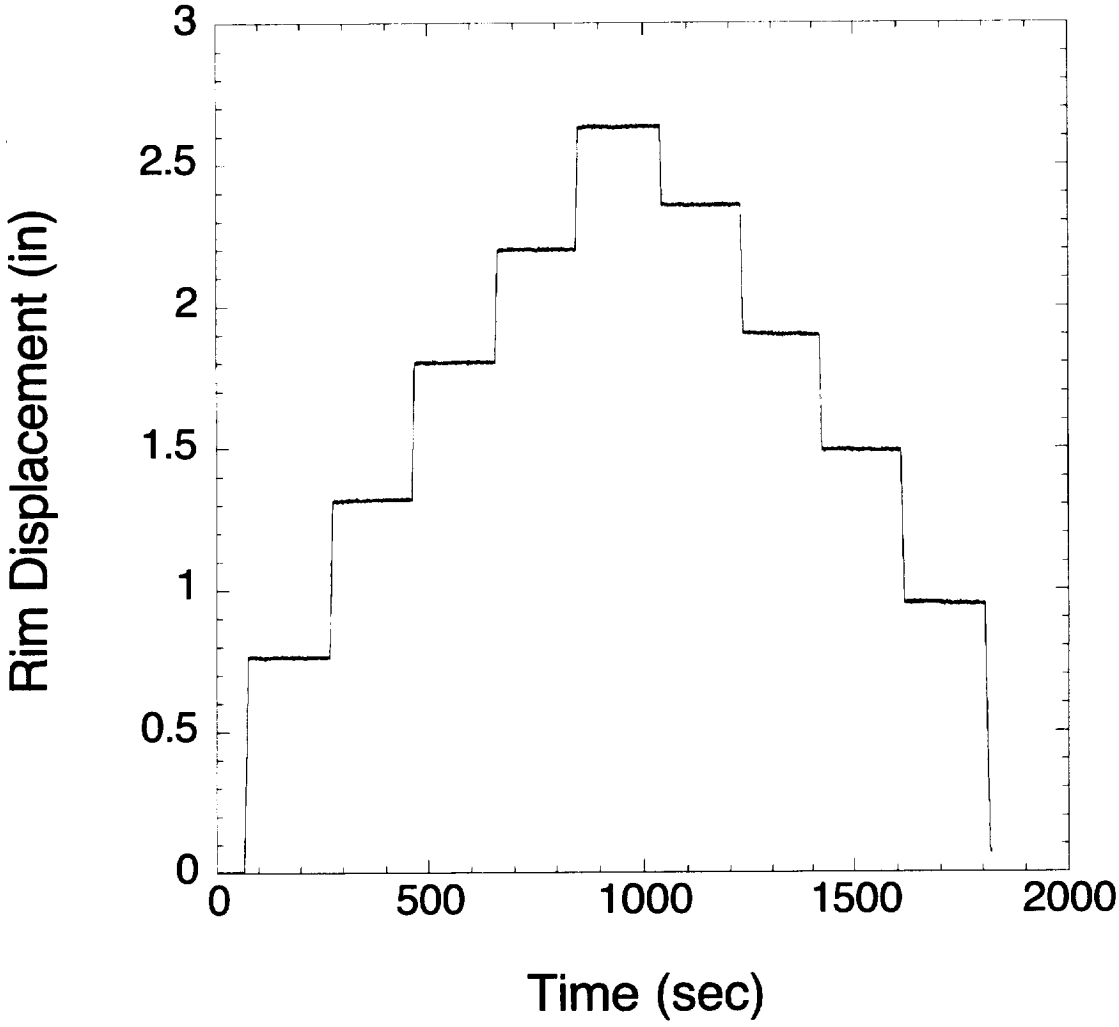

Figure 7. Measured rim displacement versus time data.

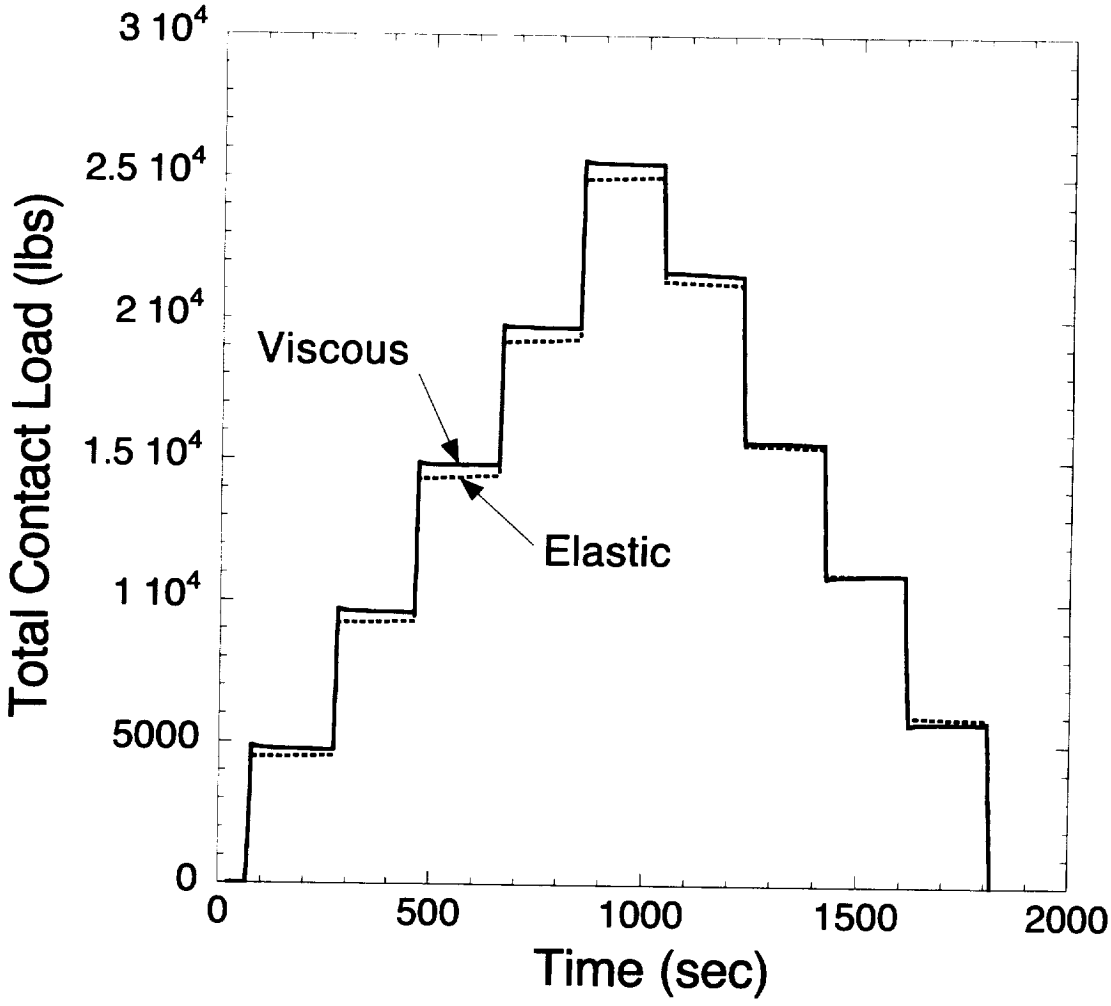

Figure 8. Viscous and elastic loads for one-dimensional stair-step simulation.

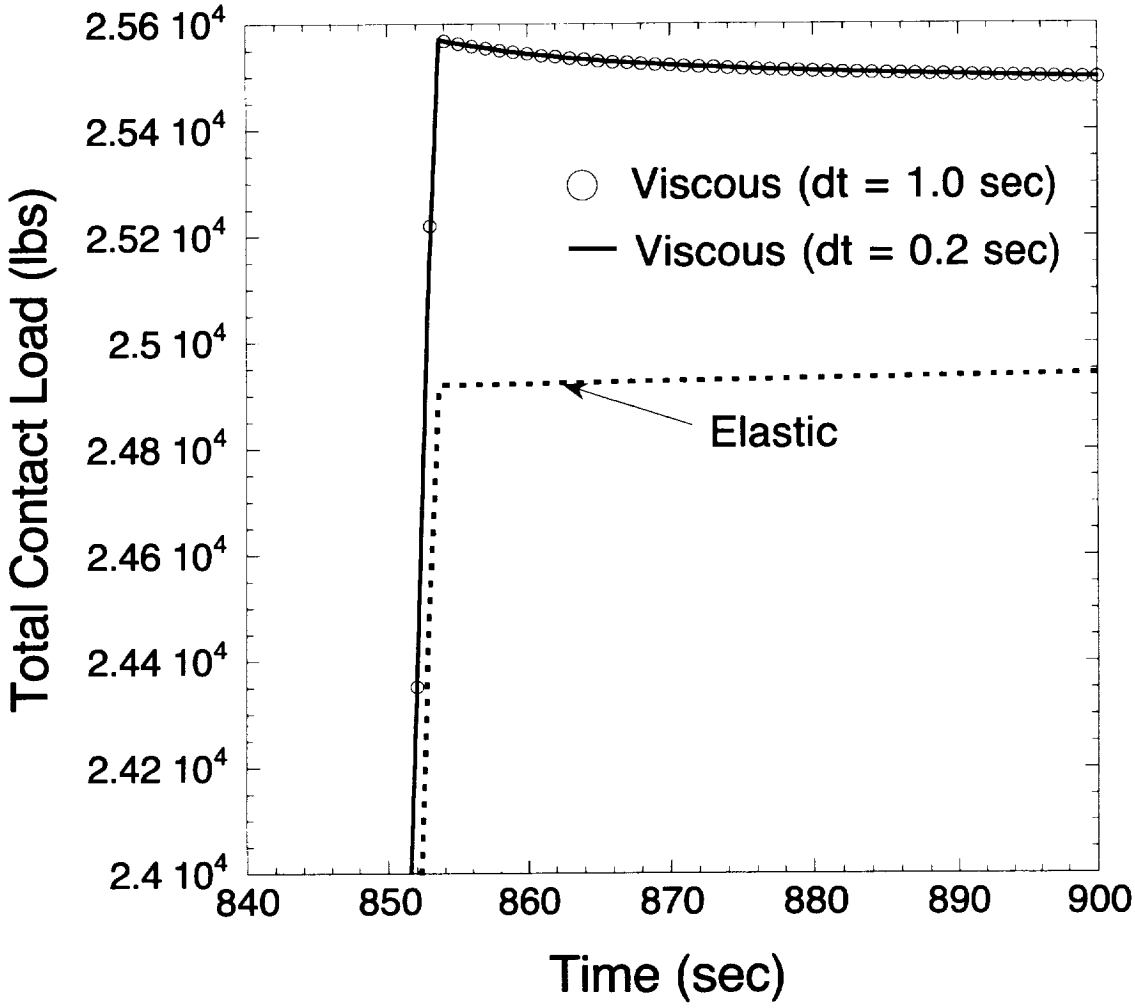

Figure 9. Computed tire loading for time steps 0.2 and 1.0 sec., one-dimensional simulation.

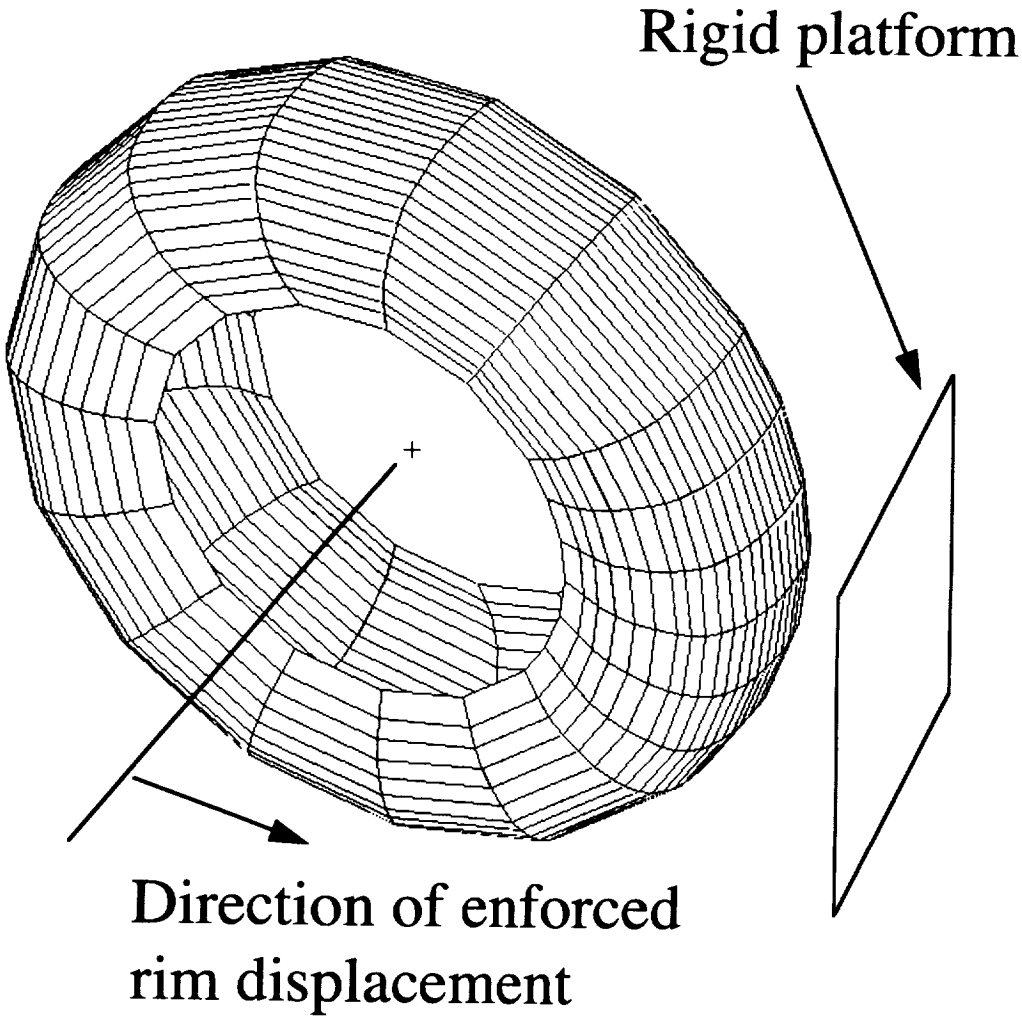

Figure 10. Tire finite element model.

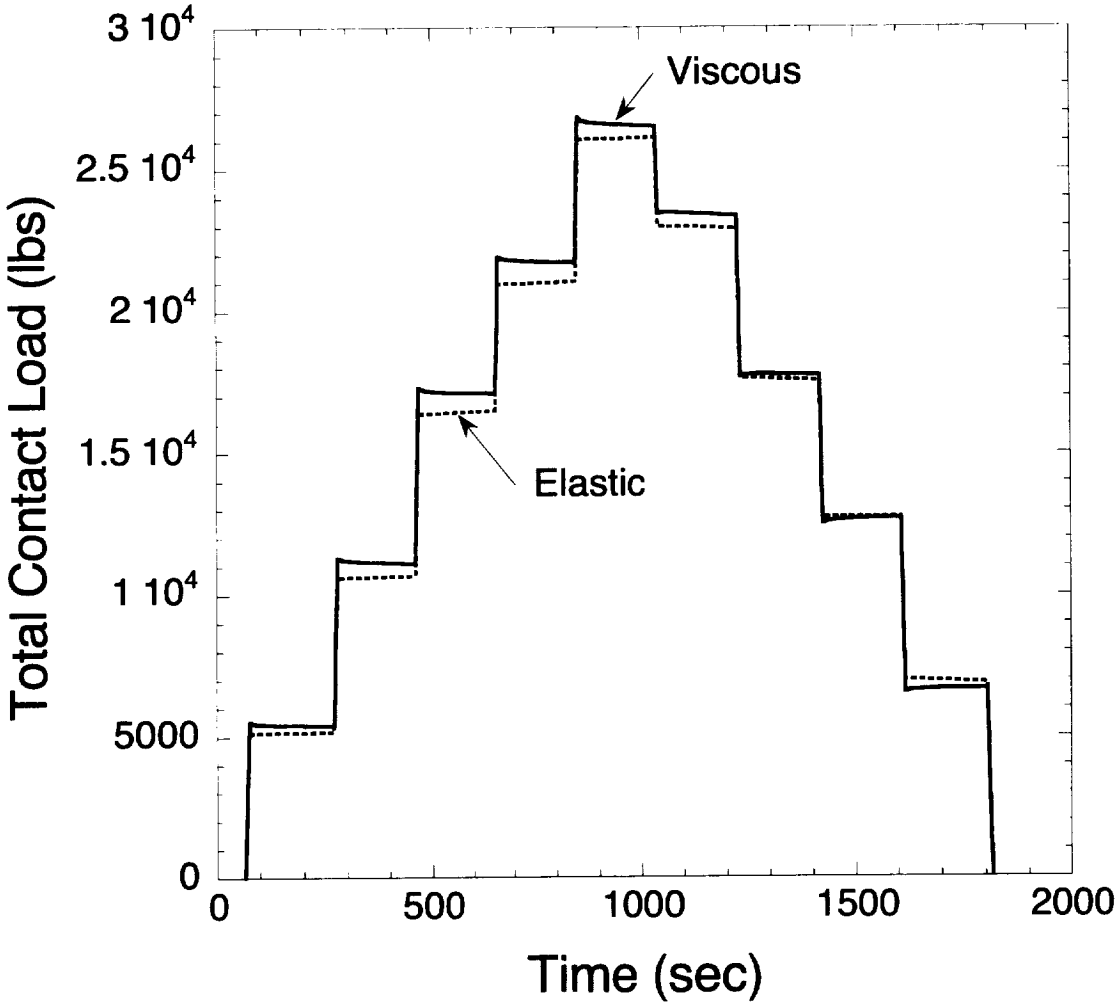

Figure 11. Viscous and elastic tire loads for finite element simulation.

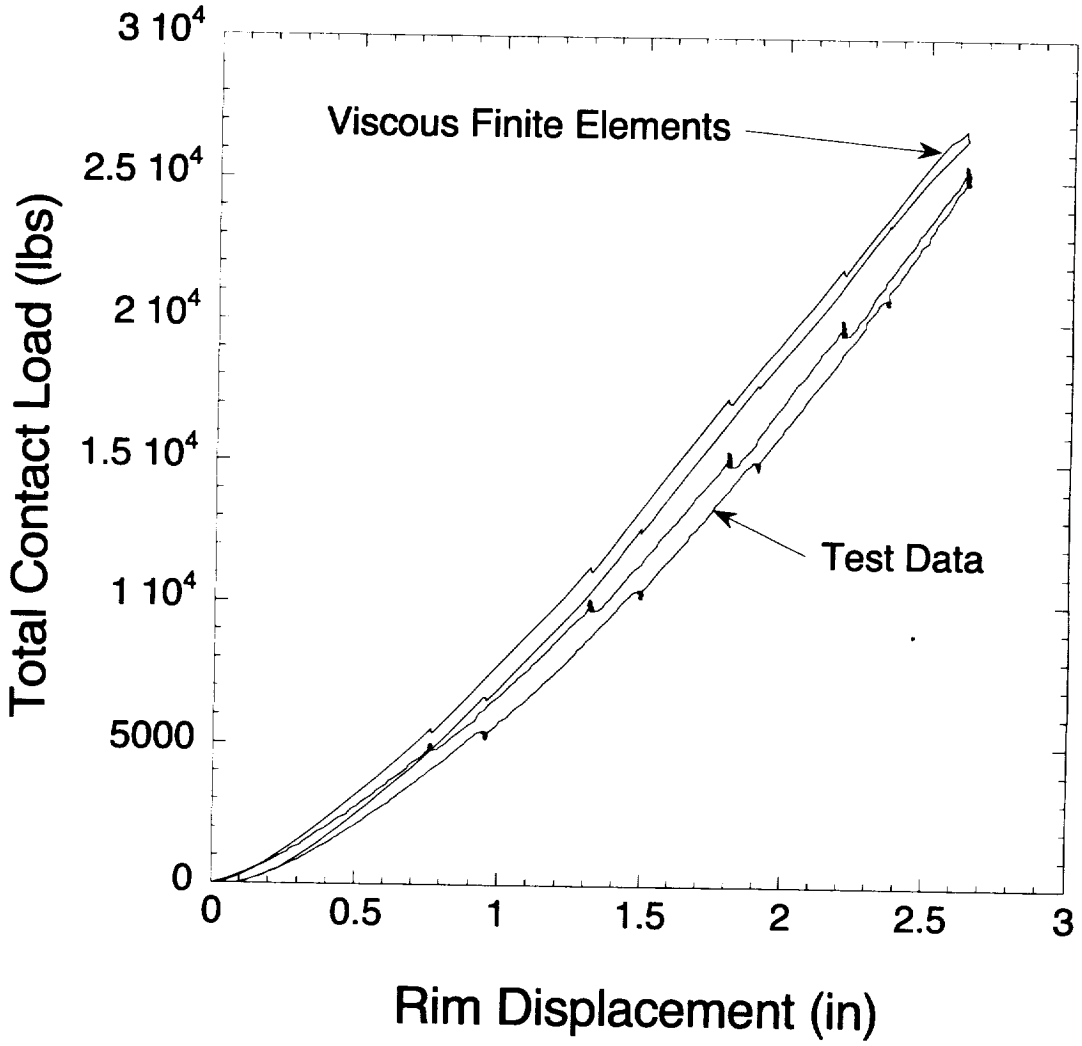

Figure 12. Finite element and test stair-step hysteresis curves.

REPORT DOCUMENTATION PAGE

Form Approved
OMB No. 0704-0188

1. AGENCY USE ONLY (Leave blank)	2. REPORT DATE	3. REPORT TYPE AND DATES COVERED
	April 1999	Technical Memorandum

4. TITLE AND SUBTITLE
Quasi-Static Viscoelastic Finite Element Model of an Aircraft Tire

5. FUNDING NUMBERS
282-10-01

6. AUTHOR(S)
Arthur R. Johnson, John A. Tanner, and Angela J. Mason

7. PERFORMING ORGANIZATION NAME(S) AND ADDRESS(ES)
NASA Langley Research Center
Hampton, VA 23681-2199

U.S. Army Research Laboratory
Vehicle Technology Directorate
NASA Langley Research Center
Hampton, VA 23681-2199

8. PERFORMING ORGANIZATION REPORT NUMBER
L-17828

9. SPONSORING/MONITORING AGENCY NAME(S) AND ADDRESS(ES)
National Aeronautics and Space Administration
Washington, DC 20546-0001
and
U.S. Army Research Laboratory
Adelphi, MD 20783-1145

10. SPONSORING/MONITORING AGENCY REPORT NUMBER
NASA/TM-1999-209141
ARL-TR-2000

11. SUPPLEMENTARY NOTES
Johnson: U.S. Army Research Laboratory, VTD, Langley Research Center, Hampton, VA; Tanner: Boeing Commercial Airplane Group, Seattle, WA,; and Mason: Langley Research Center, Hampton, VA

12a. DISTRIBUTION/AVAILABILITY STATEMENT
Unclassified-Unlimited
Subject Category 39 Distribution: Nonstandard
Availability: NASA CASI (301) 621-0390

12b. DISTRIBUTION CODE

13. ABSTRACT (Maximum 200 words)
An elastic large displacement thick-shell mixed finite element is modified to allow for the calculation of viscoelastic stresses. Internal strain variables are introduced at the element's stress nodes and are employed to construct a viscous material model. First order ordinary differential equations relate the internal strain variables to the corresponding elastic strains at the stress nodes. The viscous stresses are computed from the internal strain variables using viscous moduli which are a fraction of the elastic moduli. The energy dissipated by the action of the viscous stresses is included in the mixed variational functional. The nonlinear quasi-static viscous equilibrium equations are then obtained. Previously developed Taylor expansions of the nonlinear elastic equilibrium equations are modified to include the viscous terms. A predictor-corrector time marching solution algorithm is employed to solve the algebraic-differential equations. The viscous shell element is employed to computationally simulate a stair-step loading and unloading of an aircraft tire in contact with a frictionless surface.

14. SUBJECT TERMS
Finite Elements, Tire modeling, Viscoelasticity, Shell Theory, Shuttle

15. NUMBER OF PAGES
33

16. PRICE CODE
A03

17. SECURITY CLASSIFICATION OF REPORT	18. SECURITY CLASSIFICATION OF THIS PAGE	19. SECURITY CLASSIFICATION OF ABSTRACT	20. LIMITATION OF ABSTRACT
Unclassified	Unclassified	Unclassified	UL